PCCP

# The fast dynamics of benzene in the liquid phase

## Part II.† A molecular dynamics simulation

**R. Chelli,[ab] G. Cardini,[ab] M. Ricci,[ace] P. Bartolini,[ad] R. Righini*[abd] and S. Califano[ab]**

[a] *LENS, University of Florence, 50125 Florence, Italy. E-mail: righini@chim.unifi.it*
[b] *Department of Chemistry, University of Florence, 50121 Florence, Italy*
[c] *Department of Chemistry, University of Basilicata, 85100 Potenza, Italy*
[d] *Unità INFM Firenze*
[e] *Unità INFM Napoli*

***Received 26th January 2001, Accepted 20th April 2001***
***First published as an Advance Article on the web 25th June 2001***



A molecular dynamics simulation is performed for liquid benzene in the rigid body approximation. The results concerning the structural and dynamical properties of the system provide the basis for the interpretation of recent experimental data. In particular, it is shown that the system is characterised by a well defined cage structure, and that the average dynamics of the cages describe the main dynamical features of the bulk liquid. The calculated mean lifetime of the cages is in good agreement with the value of the Kubo correlation time derived from the experiments. In the picture emerging both from experiments and calculations, the fast intermolecular dynamics of liquid benzene is characterised by an inhomogeneously broadened distribution of intermolecular vibrational frequencies, whose dephasing is primarily due to the relaxation of the local structures. In particular, this mechanism is responsible for the dephasing of the low frequency librations giving rise to the intermediate quasi-exponential relaxation observed in the optical Kerr effect experiments.

## I Introduction

In the previous paper[1] (hereafter referred as paper I) we reported on the time resolved optical Kerr effect (OKE) investigation of the fast dynamics of benzene in the liquid phase. Besides the picosecond exponential decay due to rotational diffusion of the molecules (tumbling), at short times ($<5$ ps) the experiments show evidence of intermolecular oscillatory dynamics, and of some intermediate regime. In the interpretation proposed in paper I, in accord with the conclusions of ref. 2, we relate the oscillatory and the intermediate regimes to the inhomogeneous distribution of the intermolecular librational frequencies, and attribute the peculiar temperature-dependent shape of the intermolecular spectrum to motional narrowing effects. In this paper the dynamics of liquid benzene is investigated at a microscopic level by means of molecular dynamics (MD) simulations. MD in fact can provide basic information, not achievable with other techniques, on the structure of the liquid and on its dynamical properties at the molecular scale. Several computer simulations of liquid benzene can be found, also in recent years,[3–5] in the literature. In particular, some of us have published recently[5] the results of a MD simulation of liquid benzene. The main goal of that investigation was understanding the relaxation mechanisms of the intramolecular vibrations; however, some of the results reported there are of interest also for the description of the structure and of the rotational and translational dynamics of the liquid. Here we extend and complete that simulation, taking into account different models for the intermolecular potential, and considering the effect of changing the sample temperature; we also calculate the low frequency Raman spectral density, and compare it to the experimental optical spectra reported in paper I.

According to the results of the experimental investigation described in paper I, the most important answers we expect from the MD simulations concern the following points: (i) The translational and orientational ordering (if any) of the liquid, obviously related to the role played by the cage dynamics, as discussed in paper I; (ii) the distribution of intermolecular vibrational frequencies and, in particular, of the components corresponding to librations about in-plane axes (tumbling librations), that are expected to give the largest contribution to the optical activity; (iii) the characteristic parameters defining the cage structure and dynamics, such as its mean lifetime, to be related to the correlation time $\tau_c$ of the stochastic perturbations that appears in the Kubo treatment of the spectral line shape (see paper I); (iv) the ability of the computational method to reproduce the optical spectra obtained by Fourier transforming the time domain experimental data.

In the next section the model potential and the computational details are described. In the third section the calculated structural and dynamical properties of liquid benzene are reported and discussed and the calculated low frequency vibrational Raman spectral density is compared to the experimental results of paper I. Finally, the last section summarises some general conclusions based on the results of the present paper and on those of paper I.

## II The calculation

### The intermolecular potential

It is generally accepted that the intermolecular and intramolecular vibrations of benzene in the condensed phases are dynamically separated: the lowest intramolecular vibration in

† For Part I see ref. 1.

fact is at 404 $cm^{-1}$, far enough from any intermolecular vibrational frequency (typically lower than 200 $cm^{-1}$) to be considered completely decoupled. In ref. 5, where the main interest was in the intramolecular dynamics, a fully flexible potential model, including all the internal degrees of freedom of the molecule, was adopted. In the present paper, instead, we are interested in the intermolecular dynamics of benzene in the liquid phase, and consequently we treat the molecule as a rigid body with $D_{6h}$ symmetry. Such an assumption, adopted also in several recent and past calculations,[3,4,6–14] simplifies substantially the potential model and the dynamics of the system. It makes it also possible to treat large simulation samples, and to extend the simulation runs to relatively long times, thanks to the limited amount of data to be stored for the subsequent analysis. This last condition in particular is of crucial importance in order to achieve an acceptable signal to noise ratio of the collective correlation functions involved in the calculation of the optical properties of the sample.

Different intermolecular potential models have been used by different authors for benzene,[3–16] in most cases based on site–site interactions. In principle, the choice of the potential model may have a relevant effect on the results of the simulations; comparing the results of different potentials for the same system represents a way of assessing the degree of reliability of the calculations. Here we will consider two different models, both based on atom–atom non-bonded interactions. The LJ model, utilised for benzene in ref. 5, is based on Lennard-Jones atom–atom potentials; the B model consists of atom–atom interactions described by Buckingham-type functions. In both cases the electrostatic interactions are described by means of fractional point charges placed on the atoms. The details of the two potential models are collected in Table 1.

The LJ potential is a modified CHARMM[17] type potential, originally developed for completely flexible molecules: its intermolecular part consists of Coulombic and Lennard-Jones interactions between all pairs of non-bonded atoms. The electrostatic interactions are represented by fractional point charges of −0.115 on the carbon and 0.115 on the hydrogen. The corresponding quadrupole moment is $2.28 \times 10^{-39}$ C $m^2$, somewhat lower than the experimental value[18] of $2.9 \times 10^{-39}$ C $m^2$. In spite of this discrepancy, we preferred to retain the values of the point charges taken from the literature, since the CHARMM potential is widely referenced, and since other authors[13] have already adopted the LJ potential in the form reported in Table 1.

In the B potential the atom–atom non-bonded interactions are described by Buckingham-type functions, whose parameters were taken from ref. 7. In that paper the potential parameters were optimised for the structural and dynamical properties of crystalline benzene; the B potential then can be considered a particularly good model for the simulation of the liquid phase. The absolute value of the point charge was chosen in order to reproduce the experimental value of the quadrupole moment. We note here that the calculations reported in ref. 5 show that changing the quadrupole from 2.28 to $2.9 \times 10^{-39}$ C $m^2$ has only a very minor effect on the liquid properties; the same indication comes from the harmonic and anharmonic lattice dynamics calculations on crystalline benzene.[7]

In the experimental investigation of paper I the changes with the temperature of the decay curves and of the spectral profiles represent one of the basic points of discussion; it is then very important that also the MD simulations are performed at different temperatures, so that the predicted temperature dependence of the calculated quantities can be compared to the experimental one. As already noticed, we expect the B potential to provide a more realistic description of the intermolecular interactions in liquid benzene. We have then performed (with the procedure outlined in the next section) two simulation runs at 278 and 298 K adopting this potential. The LJ potential was employed in the room temperature simulations of ref. 5: some of the physical quantities of interest for the present investigation are therefore already available from that publication. We repeated the simulation at 278 K with the LJ model, in order to complete the set of calculated quantities and observables, and to make it possible to compare the predictions of the two different potentials.

## Computational details

All simulations were performed in the NVE ensemble (constant number of particles, volume and energy) using a cubic box of 500 molecules, with standard periodic boundary conditions. Both LJ and B potentials predict a room temperature density of the liquid almost identical to the experimental value[19] of 0.874 g $cm^{-3}$. For a better comparison of the results of the two potential models with the experimental data, we adopted a simulation box with side-length of 42 Å, corresponding to the experimental density. The very small pressures obtained in the two calculations (−0.5 atm for the LJ potential and 1.0 atm for the B potential) confirm that, in both cases, the simulated liquid is practically at the equilibrium as far as the simulation box is concerned. For all simulations a cut-off distance for the centres of mass of 14 Å was used for atom–atom and electrostatic interactions. The equations of motion were integrated with a time-step of 5 fs, using the position Verlet algorithm and the constraint method of Ciccotti and Ryckaert.[20] The rigid molecule geometry was taken from ref. 5, with the C–C and C–H bond lengths of 1.374 and 1.082 Å, respectively.

The simulations were performed at two temperatures: 278 and 298 K. The sample was initially equilibrated for 100 ps at 298 K by uniform scaling of the atomic velocities. The system was then left free to relax for the next 100 ps without velocity scaling. Finally, the coordinates and the velocities were stored for 660 ps. Starting from the last system configuration of the 298 K simulation, the sample was equilibrated at 278 K in the NPT ensemble (constant pressure, temperature and number of particles); the resulting box side-length was 41.05 Å. The system was then equilibrated in the NVE ensemble, using the

**Table 1** Parameters of the atom–atom and electrostatic potentials

| | B potential $V = A\exp(-Br) - Cr^{-6}$ | | | LJ potential $V = 4\varepsilon[(\sigma/r)^{12} - (\sigma/r)^6]$ | |
|---|---|---|---|---|---|
| | $A$/kcal $mol^{-1}$ | $B$/$Å^{-1}$ | $C$/kcal $mol^{-1}$ $Å^6$ | $\varepsilon$/kcal $mol^{-1}$ | $\sigma$/Å |
| C–C | 265834 | 3.909 | 524 | 0.070 | 3.55 |
| C–H | 8037 | 3.703 | 75 | 0.0458 | 2.985 |
| H–H | 2939 | 3.746 | 39 | 0.030 | 2.42 |
| | Atomic charge (fraction of electron) | | | Atomic charge | |
| C | −0.1345 | | | −0.115 | |
| H | 0.1345 | | | 0.115 | |

box dimension obtained from the NPT run. Finally, a production run of 760 ps was performed.

## III Results and discussion

### Structural properties

The average structural properties of liquid benzene can be described by the radial and angular distribution functions.The total radial distribution function calculated with the LJ (see Fig. 1 of ref. 5) and B (Fig. 1 of this paper) potentials are practically coincident, and follow very closely the experimental data of refs. 3 and 4. The radial distribution function of the centers of mass calculated with the B potential shows a first peak at 5.6 Å, corresponding to the first coordination shell; the peak area gives a coordination number of about 12.

The radial–angular pair distribution function provides some valuable information on the degree of orientational order in the liquid. We have computed the function

$$g(r,\theta) = \frac{1}{N\rho(r,\theta)} \left\langle \sum_i \sum_{j \neq i} \delta(r - r_{ij})\delta(\theta - \theta_{ij}) \right\rangle, \qquad (1)$$

where $\rho(r, \theta)$ is the number of molecules defined as $(N/V)2\pi r^2 \sin\theta \Delta r \Delta\theta$, $\Delta r$ and $\Delta\theta$ being the angular and radial resolution, respectively. The indices $i$ and $j$ count the molecules, and $r_{ij}$ and $\theta_{ij}$ are, respectively, the centre of mass intermolecular distance and the angle between the $C_6$ axes of the molecules $i$ and $j$. The angular brackets indicate a time average. Again, the results of the two potential models are very similar, as appears from a comparison of the plot in Fig. 2 (B potential), with the same function calculated with the LJ potential in ref. 5. It is clear that even in the first coordination shell the degree of preferential orientation is rather small; all the relative angles are accessible with similar probability, with some preference for the 90° angle. Also in this case our results agree pretty well with those reported in refs. 3 and 4. The change with temperature is small, the radial–angular distribution being slightly more uniform at high temperature. Under this respect, the structure of the "solvent" cage around any benzene molecule is largely different from that of the first neighbours in the crystal, where 8 out of the 12 closest molecules have orthogonal orientation.

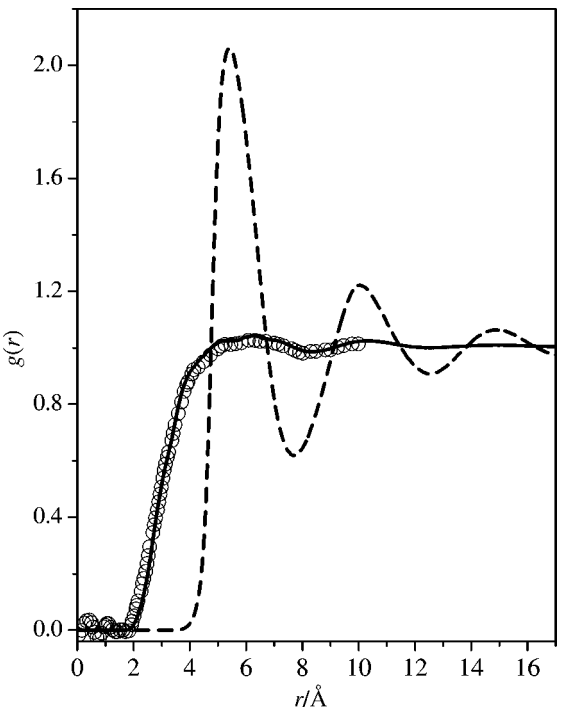


**Fig. 1** Radial distribution functions of liquid benzene calculated at 298 K (B potential). Solid line: total radial distribution function; dashed line: centre of mass radial distribution function; open circles: experimental data (from ref. 3).

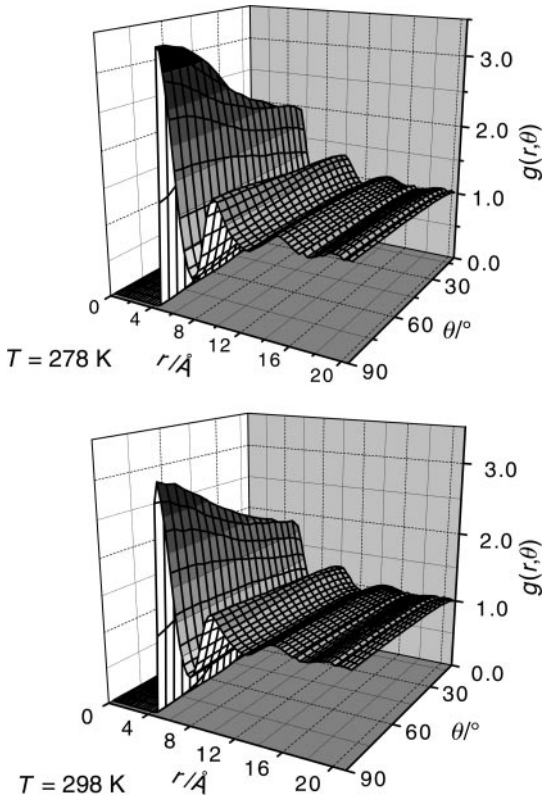


**Fig. 2** Radial–angular pair distribution function of liquid benzene at 278 and 298 K (B potential). $\theta$ is the angle between the $C_6$ axes of the molecules of the pair; $r$ is the centre of mass distance.

### Dynamical properties

The distribution of the intermolecular vibrational frequencies in the liquid can be obtained from the power spectrum (PS) of the atomic velocity autocorrelation function (ACF). The PS is closely related to the density of the vibrational states (DOS) of the liquid, weighted by the squared amplitude of motion of the atoms, and includes the effects of anharmonicity. Fig. 3 shows the PS of liquid benzene at 278 and 298 K, calculated with the B potential; the separated translational and rotational contributions are also reported. The frequency range covered by the spectrum corresponds quite closely to the width of the experimental band of Fig. 3 of paper I. It is worth noticing that both translational and librational contributions cover practically the same frequency range (from 0 to about 150 $cm^{-1}$); the shape of the rotational part, with its prominent shoulder at about 90 $cm^{-1}$, is strongly reminiscent of the experimental spectra of Fig. 3 of paper I. Similar results are obtained with the LJ potential (see ref. 5).

Additional information on the librational dynamics of the molecules can be obtained from the PS of the autocorrelation function of the angular momentum of the molecules. From the Fourier transforms of the correlation functions of the momentum components parallel and orthogonal to the $C_6$ axis it is in fact possible to obtain the frequency distribution of the librations around the $C_6$ axis (spinning librations) and around axes orthogonal to it (tumbling librations). This is a relevant separation, since the spinning motion is optically inactive for a symmetric top molecule such as benzene and, as a consequence, the librational spectra and the oscillatory OKE response depend essentially on the frequency distribution of the tumbling librations. Fig. 4 shows the two components of the power spectrum calculated at two temperatures with the B

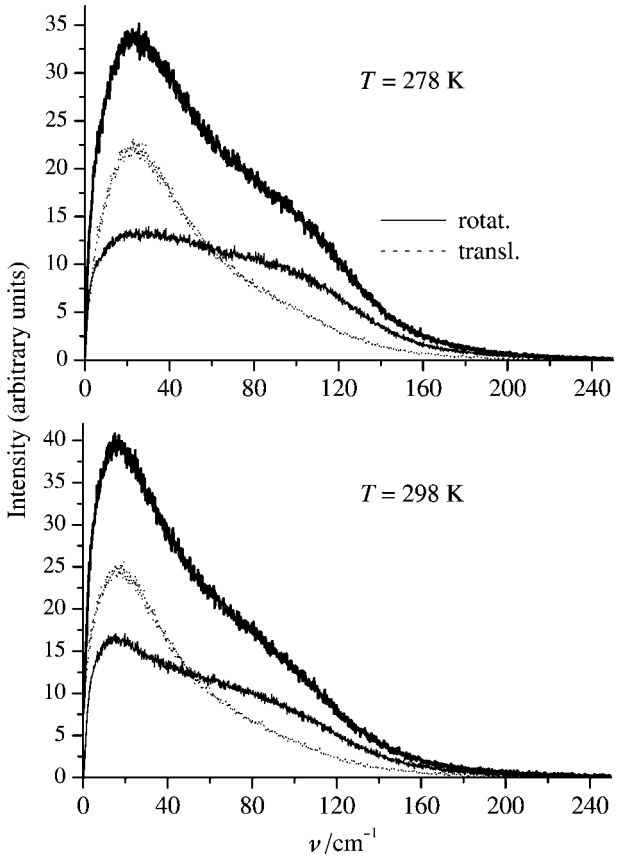


**Fig. 3** Power spectrum of the atomic velocity autocorrelation function at 278 and 298 K calculated with the B potential. The total spectrum and the translational and rotational components are shown.

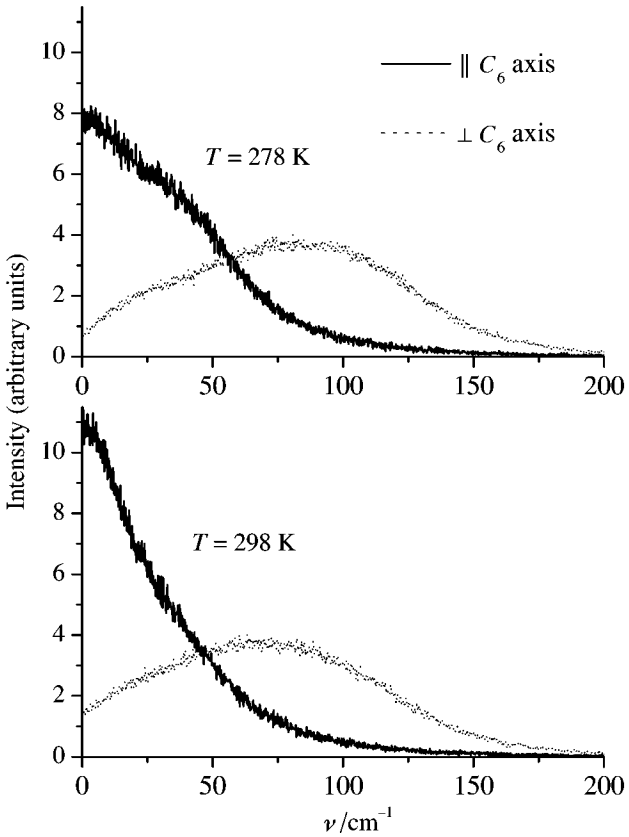


**Fig. 4** Power spectrum of the autocorrelation function of the angular momentum of benzene molecule for the B potential at 278 and 298 K. The contributions of the momentum components parallel (∥) and orthogonal (⊥) to the $C_6$ axis are shown.

potential: as expected, the parallel contribution (libration around the $C_6$ axis) is larger at low frequencies; however also the perpendicular component has a not negligible amplitude in the low frequency region. The intercept at $\omega = 0$ is indicative of the orientational diffusion, which is of course much less hindered around the symmetry axis.

In paper I, following the proposition by Loughname *et al.*,[2] we discussed the role of the stochastic perturbations (more precisely, of their correlation time $\tau_c$) in determining the shape of the spectral densities obtained from the OKE experiments, and of its temperature dependence. The emerging picture is that of a spectrum dominated by the librational motion of the molecules in their "solvent" cages. The spectral shape is determined by the inhomogeneous distribution of the tumbling librational frequencies (corresponding to the broad distribution of cage potentials), modified by motional narrowing, which affects differently the low and high frequency parts of the spectrum.

This interpretation implies that the distribution of tumbling librations has not negligible amplitude also at very low frequency, say below 25 $cm^{-1}$. The spectra in Figs. 3 and 4 may be taken as a first confirmation in this sense. More direct information on this point can be obtained by calculating the frequency spectrum of the system that we have proposed as the basic unit able to account for the main dynamic features of the liquid, *i.e.* of the molecule–cage system. The cage structure and dynamics, as predicted by the LJ potential at room temperature, have been discussed in ref. 5: here we analyse the two simulation runs performed with the B potential at the temperatures of 278 and 298 K. Briefly, the adopted procedure consists in calculating three functions:

(a) the isotropic cage deformation function

$$f_c(t) = \frac{1}{n_c}\sum_{j=1}^{n_c} R_j^2(t), \qquad (2)$$

where $n_c$ is the number of molecules in the $c$th cage, and $R_j$ is the distance between the central molecule and the $j$th molecule of the cage.

(b) The anisotropic cage deformation function

$$f_c^{[\rho\sigma]}(t) = \frac{1}{n_c}\sum_{j=1}^{n_c} \rho_j(t)\sigma_j(t) \quad \text{with } \rho \neq \sigma, \qquad (3)$$

where $\rho_j$ and $\sigma_j$ are the Cartesian components of the vector $\boldsymbol{R}_j$ joining the central molecule to the $j$th molecule of the cage.

(c) The tumbling librational function

$$f_{cj}(t) = \langle \boldsymbol{I}_{cj}(0) \cdot \boldsymbol{I}_{cj}(t) \rangle, \qquad (4)$$

consisting of the time autocorrelation function of the unit vector $\boldsymbol{I}_{cj}(t)$ parallel to the $C_6$ axis of molecule $j$ in cage $c$.

The corresponding spectra are obtained as the cosine Fourier transforms of eqns. (2)–(4). If the average is taken over all the molecules in the simulation box, the resulting spectra are completely dominated by the $\omega = 0$ diffusive contribution. As shown in ref. 5, the contribution of the oscillatory dynamics can be emphasized by restricting the averages to the "long lived" cages. The cage is then defined as consisting of the $n_c$ molecules at a distance less than 6 Å from a central molecule; when one of those molecules has diffused beyond 0.5 Å of the cage radius, the cage is considered to be destroyed. The analysis was then limited to the $N_{cg}$ cages surviving longer then 3 ps. These criteria were chosen as a good compromise between the attempt of maintaining the cage size as close as possible to the position of the first peak in the radial distribution function in Fig. 1, and the need of including in our analysis enough cages to ensure good statistics. At 278 K the long-lived cages amount to about 50% of the total; their fraction reduces to 38% at 298 K. The distribution of the number of molecules within the radius of 6 Å for the long-lived cages at 278 and 298 K, as predicted by the B potential,

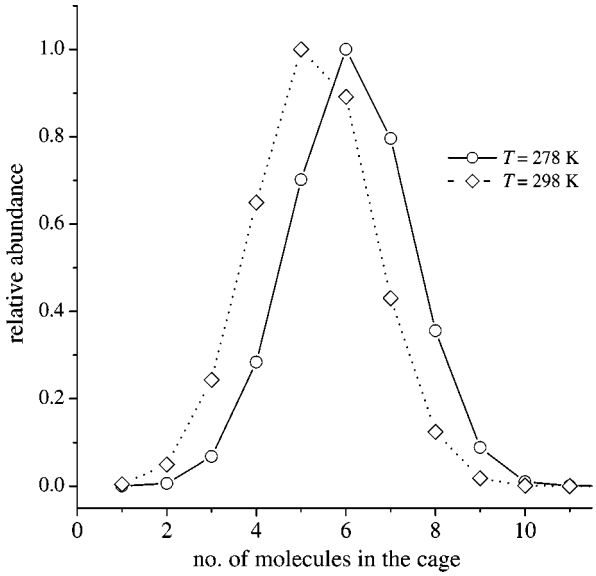


**Fig. 5** Distribution of the number of molecules laying within 6 Å from the central molecule; the average is limited to the cages living longer than 3 ps (see text). The lines are guides for the eyes. Open circles: $T = 278$ K; open diamonds: $T = 298$ K (B potential).

is shown in Fig. 5. The mean value is about 6 at the lower temperature, and decreases to 5 at room temperature.

The cage vibrational spectra are thus obtained as

$$F_{T_{\mathrm{iso}}}(\omega) = \frac{1}{N_{cg}} \sum_{c=1}^{N_{cg}} \mathscr{F}[f_c(t)] \tag{5}$$

$$F_{T_{\mathrm{aniso}}}(\omega) = \frac{1}{N_{cg}} \sum_{c=1}^{N_{cg}} \{\mathscr{F}[f_c^{[xy]}(t)] + \mathscr{F}[f_c^{[xy]}(t)] + \mathscr{F}[f_c^{[yz]}(t)]\} \tag{6}$$

$$F_{\mathrm{libr}}(\omega) = \frac{1}{N_{cg}} \sum_{c=1}^{N_{cg}} \frac{1}{n_c} \sum_{j=1}^{n_c} \mathscr{F}[f_{cj}(t)]. \tag{7}$$

The residual diffusive peak, which is still very large, can be conveniently removed by fitting a Voigt profile to the $F(\omega)$ functions of eqns. (5)–(7), and subtracting it from the original function. Fig. 6 shows the result thus obtained with the B potential at 278 and 298 K. The spectra are multiplied by $\omega$, in order to correct for the mean square amplitude factor present in the direct difference spectrum. It is quite evident the close resemblance to the densities of translational and librational states reported in Fig. 3. This is, first of all, an important confirmation that the basic unit consisting of a molecule in the cage actually accounts for the dynamical properties (at least on the short time scale considered here) of the bulk liquid. It is also in accord with the assumption of Ratajska-Gadomska *et al.*,[21] who obtained the intermolecular frequencies of liquid benzene on the basis of a quasi-crystalline structure of the first neighbours. An important point in the interpretation of the OKE experiments given in paper I, is the assumption that the spectra are essentially determined by the frequency distribution of the tumbling librations. The spectra of Fig. 6 confirm that the distribution of those frequencies covers the entire spectral range of interest, with large amplitude also in the very low frequency region. In this respect, it has to be stressed that the broad distribution of librational frequencies in Fig. 6 originates from a single molecular "mode", namely the libration around an in-plane axis, and that such a broad spectrum can be attributed to a correspondently broad distribution of cage potential wells. In summary, the results of Fig. 6, together with those of Figs. 3 and 4, provide good support to the conclusions of paper I,

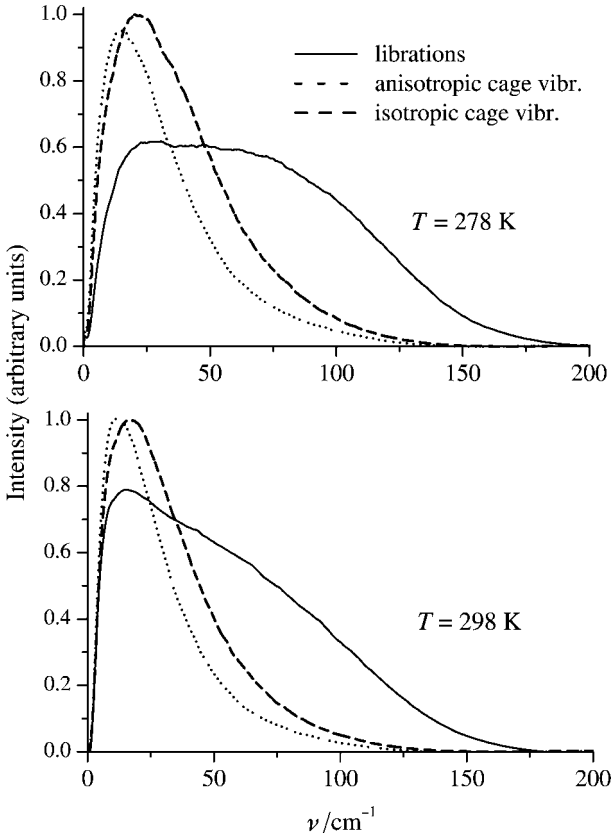


**Fig. 6** Frequency spectra obtained by Fourier transformation of the cage vibrational functions defined in the text. Solid line: spectrum of the librations about in-plane axes (tumbling librations); dotted line: spectrum of the anisotropic cage deformation; dashed line: spectrum of the isotropic cage deformation. Only "long lived" cages were included in the analysis (see text).

based on the inhomogeneous origin of the spectral line shape and the motional narrowing of the low frequency components in liquid benzene.

In that picture a key role is played by the rate of the stochastic perturbations, *i.e.* by the correlation time $\tau_c$. Since at very short delay times the molecular motion consists prevalently of oscillations in the cage potential, it is quite natural to assume that a close relation exists between $\tau_c$ and the cage lifetime. Of course there is no obvious way of defining such a lifetime; the MD simulation however makes it possible to follow the time evolution of the first neighbours around any tagged molecule, and to calculate the relaxation time of some quantity that can be reasonably related to such a lifetime. In ref. 5 a procedure was proposed, based on the definition of a time dependent $N$ dimensional ($N$ being the number of molecules in the simulation box) quantity $\boldsymbol{L}_n(t)$, the "cage status" vector, associated to each molecule $n$. Each of the $N$ components of $\boldsymbol{L}_n(t)$ can be 0 or 1. If a molecule $m$ lay within a specific cage radius from the molecule $n$, the component $m$ of $\boldsymbol{L}_n(t)$ is 1: otherwise, the component is 0. The component $n$ of $\boldsymbol{L}_n(t)$ is assumed as always 0. The time evolution of the autocorrelation of this "cage status" vector

$$C(t) = \frac{1}{N} \sum_{n=1}^{N} \langle \boldsymbol{L}_n(t) \cdot \boldsymbol{L}_n(0) \rangle \tag{8}$$

measures the average time needed by the molecules to leave the cage. In order to suppress artifacts due to back-diffusion effects, we have imposed the condition that when a molecule leaves the cage, it is not allowed to return. In Fig. 7 is shown the time evolution of $c(t)$ of eqn. (8), calculated with the B potential at two temperatures, adopting for the cage radius the value of 5.6 Å corresponding to the first peak of the centre

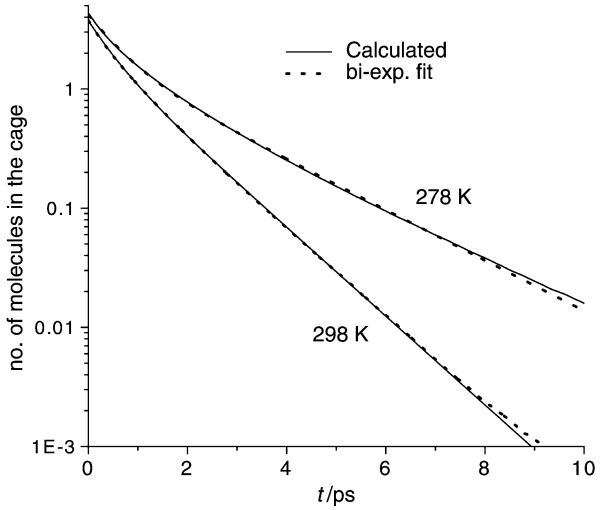


**Fig. 7** Time evolution of the "cage status" autocorrelation function (see text) at 278 and 298 K (B potential). The curves provide an estimate of the cage lifetime.

**Table 2** Relaxation times ($\tau'$, $\tau''$) and pre-exponential factors ($a'$, $a''$) of the bi-exponential fit of the "cage status" autocorrelation function (see text). The function fit is: $f(t) = a' \exp(-t/\tau') + a'' \exp(-t/\tau'')$

| | B potential | | LJ potential |
|---|---|---|---|
| | $T = 278$ K | $T = 298$ K | $T = 298$ K |
| $a'$ | 2.4 | 1.6 | 1.33 |
| $\tau'$/ps | 0.59 | 0.45 | 0.38 |
| $a''$ | 1.8 | 2.1 | 2.21 |
| $\tau''$/ps | 2.05 | 1.17 | 1.12 |

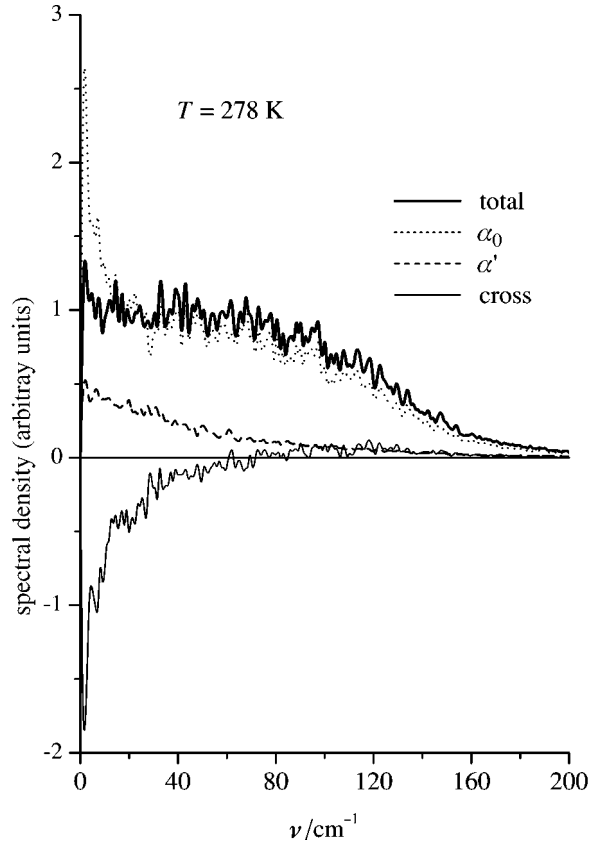


**Fig. 8** Raman spectral density (thick solid line) calculated by Fourier transforming the time autocorrelation function of the collective polarisation at 278 K. The contributions of the static polarisability (dotted line), of the induction term (dashed line) and of the cross term (thin solid line) are shown.

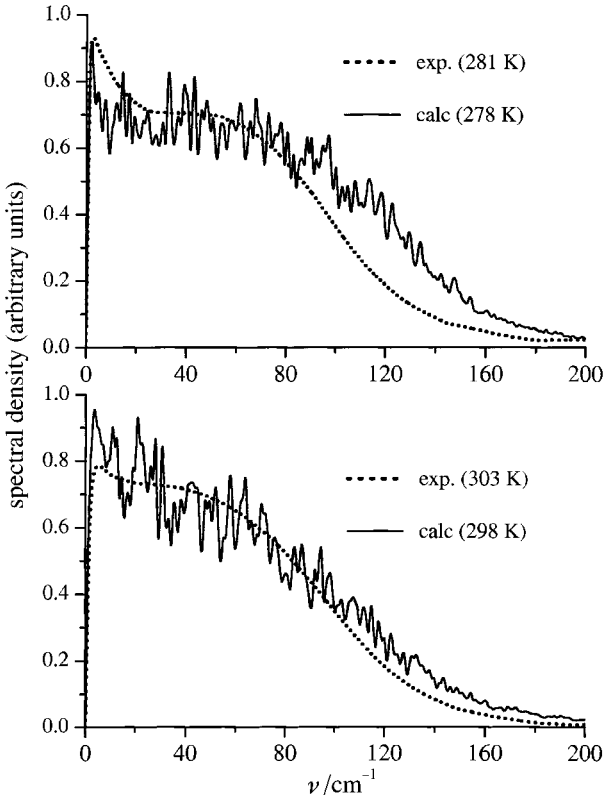


**Fig. 9** Comparison of the calculated and experimental Raman spectral densities at different temperatures (B potential).

of mass radial distribution function (Fig. 1). The curves in Fig. 7 are well fitted by a bi-exponential function, whose parameters are given in Table 2, where the fit parameters obtained with the B potential are compared to those given by the LJ model at 298 K. The two sets of results are quite similar, once more confirming that our findings are not critically affected by the choice of the intermolecular potential.

In all cases the 5.6 Å cage consists, in average, of about four molecules; about half of them (the number changes with the temperature) escape the cage rather quickly ($\tau'$ of the order of half a picosecond), while a longer time $\tau''$ is needed for the remaining molecules to leave the cage. We believe that the short times $\tau'$ of Table 2 can be taken as good reference values for the correlation time $\tau_c$ of Kubo theory. More precisely, $\tau'$ should be considered as an upper limit to the "true" value of the inverse rate of the stochastic perturbations; in fact, our

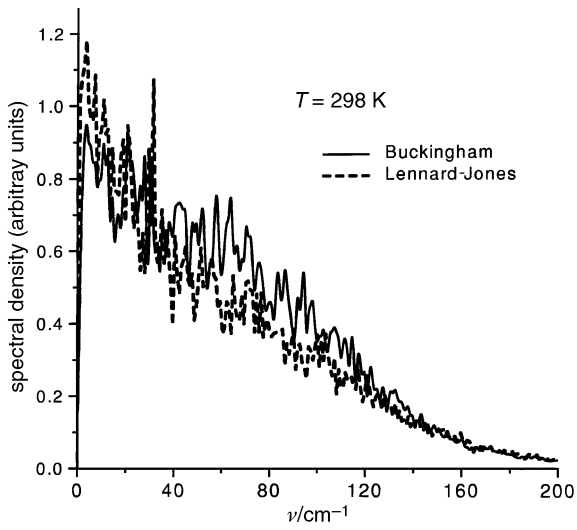


**Fig. 10** Raman spectral density at 298 K calculated with the B and LJ potentials.

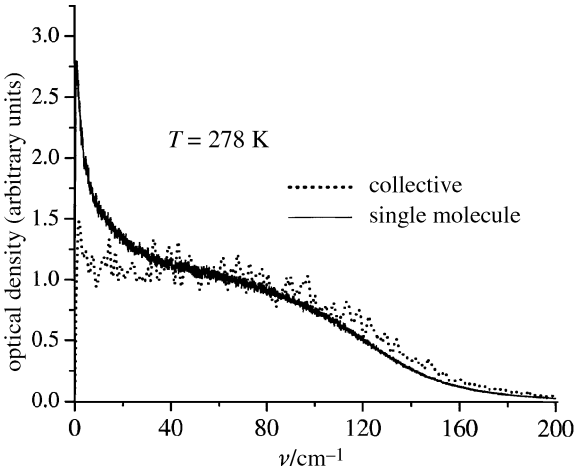


**Fig. 11** Calculated Raman spectral density of benzene at 278 K (B potential). Solid line: Fourier transform of the single molecule polarisation; dotted line: Fourier transform of the collective polarisation.

definition of cage lifetime does not include the effects due to flipping or large amplitude rotations of the molecules in the cage. In this respect, the values of $\tau'$ are fully consistent with the value of $\tau_c$ estimated by us in paper I, on the basis of the Kubo interpretation of the OKE experimental data. Also its temperature dependence is the correct one for explaining the motional narrowing effect invoked as an explanation of the changes with temperature of the spectral shape, and of the appearance of the fast exponential decay in the OKE time domain data.

### Raman spectral density

The optical response of liquid benzene can be calculated from the time autocorrelation function of the sample polarisation $\Pi$. In turn, $\Pi$ can be expressed in terms of the molecular polarisability $\alpha$,

$$\Pi = \sum_n \alpha_n, \tag{9}$$

where the induction effects are included by means of the expression

$$\alpha_n = \alpha_n^0 + \alpha_n' = \alpha_n^0 + \sum_{m \neq n} \alpha_n^0 \, \boldsymbol{T}_{nm} \, \alpha_m^0; \tag{10}$$

the sum runs over all the $m$ molecules different from $n$, $\boldsymbol{T}_{mn}$ is the dipole interaction tensor between molecules $m$ and $n$ and $\alpha_n^0$ is the polarisability of the isolated molecule.

The time dependent nuclear response function in an OKE experiment is proportional to the time derivative of the autocorrelation function of the off-diagonal elements of the polarisation tensor $\Pi$:

$$R^{(\beta\gamma)}(t) = -\frac{1}{K_B T}\,\theta(t)\,\frac{\mathrm{d}}{\mathrm{d}t}\,\langle \Pi_{\beta\gamma}(t)\Pi_{\beta\gamma}(0)\rangle, \tag{11}$$

where $\beta\gamma = xy,xz,yz$, and $\theta(t)$ is the Heaviside step function.

In an isotropic liquid the three spatial directions are equivalent, and the response function $R(t)$ is obtained from eqn. (11) by averaging on the off-diagonal components.

From the Fourier transform of the nuclear response function

$$\chi(\omega) = \int_{-\infty}^{\infty} R(t)\, \mathrm{e}^{-i\omega t}\, \mathrm{d}t \tag{12}$$

we finally obtain the spectral density $S(\omega)$ as the imaginary part of $\chi(\omega)$

$$S(\omega) = \mathrm{Im}[\chi(\omega)]. \tag{13}$$

Fig. 8 shows the spectral density obtained from the 278 K simulation; the different contributions from $\alpha^\circ$, $\alpha'$ and from the cross term are also reported. As already observed for other molecular liquids,[22–26] the induction term $\alpha'$ is almost cancelled by the negative contribution of the cross term, which also significantly reduces the intensity of the strong peak at $\omega \approx 0$ originated from the $\alpha^\circ$ term.

In Fig. 9 the spectral densities calculated at 278 and 298 K are compared with the experimental spectra. Since the corresponding time ACF are quite noisy, it is not possible to reliably identify and subtract the long time exponential decay due to rotational diffusion; the calculated spectra then contain also the sharp peak due to this kind of motion, and then have to be compared to the "full" spectra of Fig. 3a in paper I. The overall shape of the experimental data is well reproduced, although the calculated band extends too high in frequency. This is an indication that the cage potential predicted by the B potential model is slightly too stiff. The same spectra calculated with the LJ potential have similar shape: although they are slightly less structured in the high frequency part, they cover essentially the same frequency range (see Fig. 10).

As a comparison, we have also calculated the average single molecule ACF $\langle\alpha(t)\alpha(0)\rangle$, adopting the same definition of eqn. (10) for $\alpha$. Also in the case of the single molecule spectrum obtained by Fourier transforming this correlation function, the $\alpha^\circ$, $\alpha'$ and cross term contribute to the overall intensity profile in the same manner as shown in Fig. 8. However, the total spectrum differs remarkably from the collective one: as shown in Fig. 11, while the high frequency part is practically the same, the low frequency peak is strongly enhanced in the single molecule spectrum. This is likely to be a real effect: we already mentioned in paper I that the experimental spectra of benzene in $CCl_4$ (Fig. 5 of paper I), which can be taken as a good approximation to single molecule spectra, show a rather pronounced low frequency peak.

## IV Conclusions

The molecular dynamics simulations, together with the experimental results discussed in paper I, provide a sound basis for a reliable description of the structural and dynamical properties of liquid benzene that can be summarised in the following points.

From the structural point of view, the liquid is characterised, at short range, by a well defined distribution of "solvation" shells. The orientational order is instead much less pronounced, with a slight preference for the orthogonal orientation of the molecules in the first neighbor's shell.

The fast dynamics of the system corresponds to a density of intermolecular vibrational states, translational and librational in character, extending from zero to about 150 $cm^{-1}$, in good agreement with the Raman spectral density obtained from the OKE experiments. Furthermore, we have shown that the main vibrational features of the system are well reproduced also by considering the average dynamics of individual "cages", consisting of a tagged molecule surrounded by its first solvation shell. This represents an important support to the interpretation of the experimental data proposed in paper I, and of the inhomogeneous nature of the width of the intermolecular vibrational band obtained from the OKE data.

The mean lifetime of the cages, as derived from the analysis of the MD simulation, is in good agreement with the value of the perturbation correlation time derived in paper I from the Kubo analysis of the experimental vibrational spectra. This supports the idea that the relaxation of the local structures is the main source of dephasing in this kind of molecular liquid. In particular, this relaxation mechanism is responsible for the dephasing of the low frequency tumbling librations giving rise to the intermediate quasi-exponential relaxation observed in the OKE experiments. We notice here that the agreement between the results obtained with two different intermolecular

potential models confirm that our conclusions are not strongly model-dependent, and that our simulations provide a reliable description of the structural and dynamical properties of liquid benzene.

Finally, we have shown that the Fourier transform of the collective autocorrelation function of the sample polarization, obtained by including induction effects in the molecular polarisability, reproduces remarkably well the shape of the experimental Raman spectral density, and its temperature dependence.

## Acknowledgements

This work was supported by the EU under contracts ERB-FMGE-CT950017 and HPRI-CT1999-00111, and by the Italian Ministero dell'Università e Ricerca Scientifica (MURST).

## References

1 M. Ricci, P. Bartolini, R. Chelli, G. Cardini, S. Califano and R. Righini, *Phys. Chem. Chem. Phys.*, 2001, **3**, 2795.
2 B. J. Loughname, A. Scodinu, R. A. Farrer, J. T. Fourkas and U. Mohanty, *J. Chem. Phys.*, 1999, **111**, 2686.
3 M. I. Cabaço, Y. Danten, M. Besnard, Y. Guissani and B. Guillot, *J. Phys. Chem. B*, 1997, **101**, 6977.
4 T. Tassaing, M. I. Cabaço, Y. Danten and M. Besnard, *J. Chem. Phys.*, 2000, **113**, 3757.
5 R. Chelli, G. Cardini, P. Procacci, R. Righini, S. Califano and A. Albrecht, *J. Chem. Phys.*, 2000, **113**, 6851.
6 D. J. Evans and R. O. Watts, *Mol. Phys.*, 1976, **32**, 93.
7 S. Califano, R. Righini and S. H. Walmsley, *Chem. Phys. Lett.*, 1979, **64**, 491.
8 O. Steinhauser, *Chem. Phys.*, 1982, **73**, 155.
9 M. Claessens, M. Ferrario and J. P. Ryckaert, *Mol. Phys.*, 1983, **50**, 217.
10 F. Serrano Adan, A. Banon and J. Santamaria, *Chem. Phys.*, 1984, **86**, 433.
11 P. Linse, *J. Am. Chem. Soc.*, 1984, **106**, 5425.
12 P. Linse, S. Engström and B. Jönsson, *Chem. Phys. Lett.*, 1985, **115**, 95.
13 W. L. Jorgensen and D. L. Severance, *J. Am. Chem. Soc.*, 1990, **112**, 4768.
14 C. J. Craven, P. D. Hatton and G. S. Pawley, *J. Chem. Phys.*, 1993, **98**, 8244.
15 J. Anderson, J. J. Ullo and S. Yip, *J. Chem. Phys.*, 1987, **86**, 4078.
16 T. Nakagawa, J. Umemura, S. Hayashi, M. Oobatake, Y. Miwa and K. Machida, *Mol. Phys.*, 1996, **88**, 1635.
17 B. R. Brooks, R. E. Bruccoleri, B. D. Olafson, D. J. States, S. Swaminathan and M. Karplus, *J. Comput. Chem.*, 1983, **4**, 187.
18 C. G. Gray and K. E. Gubbins, *Theory of molecular fluids*, Clarendon, Oxford, 1984.
19 *CRC Handbook of Chemistry and Physics*, CRC Press, Boca Raton, 1997–1998.
20 G. Ciccotti and J. P. Ryckaert, *Comp. Phys. Rep.*, 1986, **4**, 345.
21 B. Ratajska-Gadomska, W. Gadomski, P. Wiewior and C. Radzewicz, *J. Chem. Phys.*, 1998, **108**, 8489.
22 T. Keyes, D. Kivelson and J. P. McTague, *J. Chem. Phys.*, 1971, **55**, 4096.
23 D. Frenkel and J. P. McTague, *J. Chem. Phys.*, 1980, **72**, 2801.
24 L. C. Geiger and B. M. Ladanyi, *J. Chem. Phys.*, 1987, **87**, 191.
25 L. C. Geiger and B. M. Ladanyi, *J. Chem. Phys.*, 1989, **91**, 2764.
26 H. Torii and M. Tasumi, *J. Phys. Chem. A*, 2000, **104**, 4174.